Front. Earth Sci. 2022, 16(3): 568–586
https://doi.org/10.1007/s11707-021-0943-4

RESEARCH ARTICLE

Geochemical investigation of low latitude black shale intervals of the Lower to Middle Jurassic succession, Indus Basin, Pakistan

Fahad ALI[1,2], Shiqi ZHANG (✉)[1], Muhammad HANIF[3], Mohibullah MOHIBULLAH[4], Yaxuan ZHANG[5], Muhammad USMAN[1], Sheng WANG[6], Xueliang LIU[6], Pengjie MA[1], Dongmou HUANG[1]

1 School of Geosciences, China University of Petroleum (East China), Qingdao 266580, China
2 Department of Geology, Bacha Khan University, Charsadda 24430, Pakistan
3 National Centre of Excellence in Geology, University of Peshawar, Peshawar 25000, Pakistan
4 Department of Geology, University of Balochistan, Quetta 87300, Pakistan
5 School of geosciences, The University of Edinburgh, Edinburgh, EH8 9JU, UK
6 Lukeqin Oil Production Plant, PetroChina Tuha Oilfield, Turpan City 828202, China

Abstract The Lower to Middle Jurassic sedimentary succession is dominated by siliciclastics with a significant amount of black shales in the Indus Basin, Pakistan. Several outcrop samples have been studied using an integrated approach to interpret the conceptual depositional setting from carbon and oxygen isotopes ($\delta^{13}C$ & $\delta^{18}O$), organic geochemistry, and palynofacies with major and trace element analysis. For interpretation of trace element data, various single and elemental ratios have been used in this research to unlock the geological history of the studied strata. Ti/Al is 1.96 for high-potential source rock and 7.82 for non-potential source rock, and Cr (less than 1) indicates low clastic input with low oxygen for stratified and stagnant water. The ratios of V/(V + Cr), V/(V + Ni), V/Mo, V/Ni, (Cu + Mo)/Zn, Mo/Al, isotopic values of $\delta^{13}C$ and $\delta^{18}O$ and besides the V/Cr elemental ratio, all proxies indicate that there are oxygen-depleted anoxic conditions at high potentials, while in non-potential source rock, these ratios show oxic to sub-oxic settings. In addition to the trace element correlation with total organic carbon, the influx of organic matter is determined by the palynoafacies analysis, which indicates mixed terrestrial and marine organic influx in high-potential source rock and vice versa. Furthermore, the studies of palynofaceis DFPF A-D and SFPF A-B suggest that the depositional setting of black shale occurred in the anoxic proximal to distal shelf. The results suggest that the regional and local occurrence of black shale during the Lower to Middle Jurassic and its geological condition were addressed, and these play an important role in its depositional and paleooceanographic setting in the Eastern Tethys.

Keywords black shale, Jurassic, trace elements, organic matter, Indus Basin, Pakistan

1 Introduction

The black shale has been considered as a variety of fine-grained, organic-rich source rocks deposited in a wide range of geological settings (Waples, 1983; Bohacs et al., 2000). The geological settings for organic-rich sediments range from freshwater-estuarine to marine and incorporate varying organic productivity, sedimentary pH values, and anoxia (Vine and Tourtelot, 1970; Chen et al., 2013). The black color of shales in the deposited setting is not only due to the presence of high organic matter under anoxic or reducing conditions but also the presence of common microcrystalline sulfide compounds, such as FeS (black) or FeS_2 (green) and black minerals (Mn) (Chen et al., 2013). The investigation of the bulk composition of black shales and mud shows pre-erosional source rocks, the chemistry of the depositional environment, and post-lithification processes in the reservoir and source settings (Quinby-Hunt and Wilde, 1994). The bulk composition of sedimentary rocks varies due to the physical-chemical conditions of the depositional setting (Usman et al., 2020a, 2020b, 2020c), such as the presence of organic matter, isotope signals, major and trace elements anomalies (Brumsack, 2006; Piper and Calvert, 2009; Baioumy and Ismael, 2010). The deposition of black shale is present

Received January 27, 2021; accepted August 15, 2021

E-mail: shqzhang@upc.edu.cn

across the globe during the Lower to Middle Jurassic era (Fig. 1). In the case of the Indus Basin, the previous researchers have addressed the subject of the conventional sedimentology and stratigraphy of Mesozoic carbonate and clastic units (Fatmi et al., 1990; Ahmed et al., 1997; Abbasi et al., 2012; Ali et al., 2019; Iqbal et al., 2019; Mensink et al., 1988; Mertmann and Ahmad, 1994). Besides the conventional sedimentology, Ali et al. (2018) has studied the anoxic events in the Indus Basin, Pakistan. Overall, research about the depositional setting and paleooceanographic setting of Lower to Middle Jurassic shale in the Indus Basin, Eastern Tethys, is scarce to absent. To obtain insight into the local and regional black shales and paleoenvironmental changes, an integrated study has been conducted using the trace element anomalies, palynofacies, source rock geochemistry, and carbon and oxygen isotope ($\delta^{13}C$ & $\delta^{18}O$) measurements. The results of this study will lead to the development of a conceptual depositional model and paleooceanographic implications of the Lower to Middle Jurassic shale of the Indus Basin.

2 Geological setting of Jurassic succession

The study area is located in the Indus Basin in Pakistan, which has been divided into the Lower, Middle, and Upper Indus Basins. Geologically, the Upper Indus Basin is a complex terrain that is further divided into Potwar and Kohat sub-basins in the east and the west, respectively (Kadri, 1995). The Indus Basin contains late Precambrian to Quaternary sedimentary rocks (Shah, 2009) with moderate to thick sedimentary successions (Fig. 2). The Mesozoic strata are represented by clastic and carbonate rocks such as sandstone, organic black shale, limestone, dolomite, coal, marls, and subordinate chert and laterite. The Jurassic rocks are represented by the Datta, Shinawari, and Samana Suk formations in the Upper Indus Basin with the Shirinab, Chiltan, and Mazar Drik formations in the Lower Indus Basin (Bender and Raza, 1995; Kadri, 1995; Shah, 2009). The Jurassic strata largely constitute a thick succession (820 m in the Upper Indus Basin and 3000 m in the Lower Indus Basin) of clastic and carbonate sedimentary rocks (Kazmi and Jan, 1997), and extend all along the Indus Basin from platform cover to the Kirthar-Sulaiman region, Balochistan-ophiolite, and Himalayan fold and thrust belt. In the Kirthar-Sulaiman region, they are present in the core of the anticline, whereas in Balochistan, the ophiolite and thrust belt and the Himalayan fold and thrust belt form extensive thrust blocks or sheets. A maximum thickness of approximately 3000 m is recorded in the Sulaiman-Kirthar fold-thrust belts, which consist mainly of limestones and subordinate shale of the Shirinab Formation (equal to the Ferozabad Group), Takatu/Chiltan, and Mazar Drik Formations (Kazmi and Jan, 1997).

The deposition of the Lower Jurassic strata in the Indus Basin, Pakistan, is mainly influenced by tectonics, but the role of paleoclimate changes cannot be ignored. The

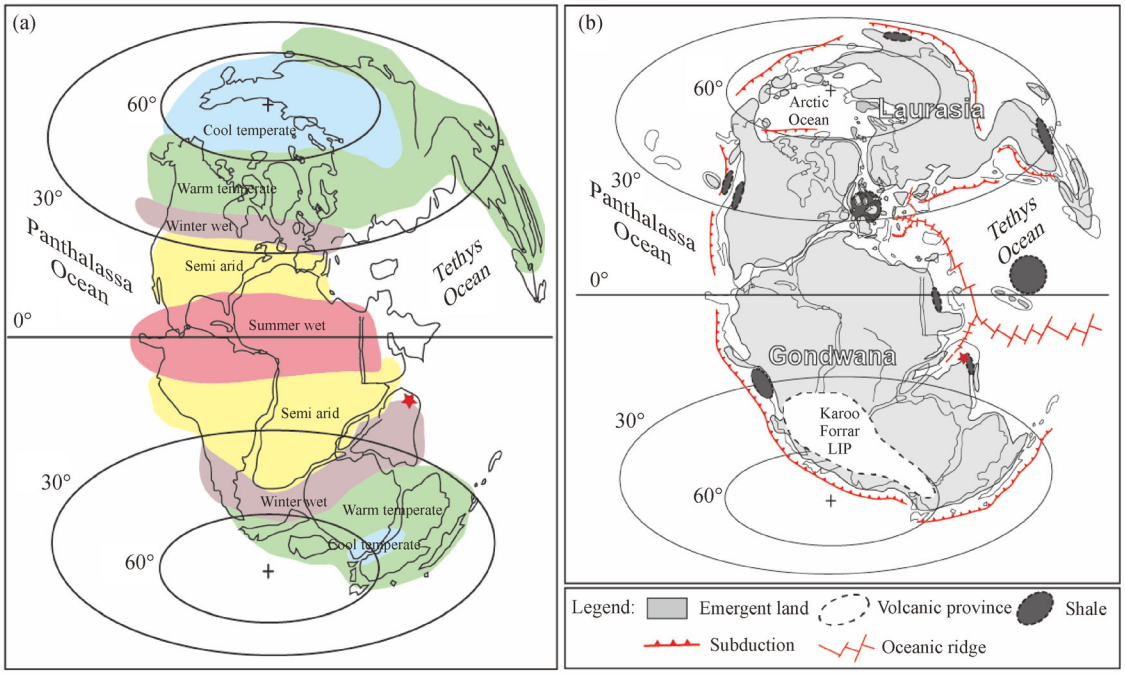

Fig. 1 The location of the Indus Basin (is shown by the red color star). (a) Lower Jurassic paleo-geography and paleo-climatic belts (Rees et al., 2000; Dera et al., 2009); (b) the area of deposition of black shale across the globe (Ikeda et al., 2018).

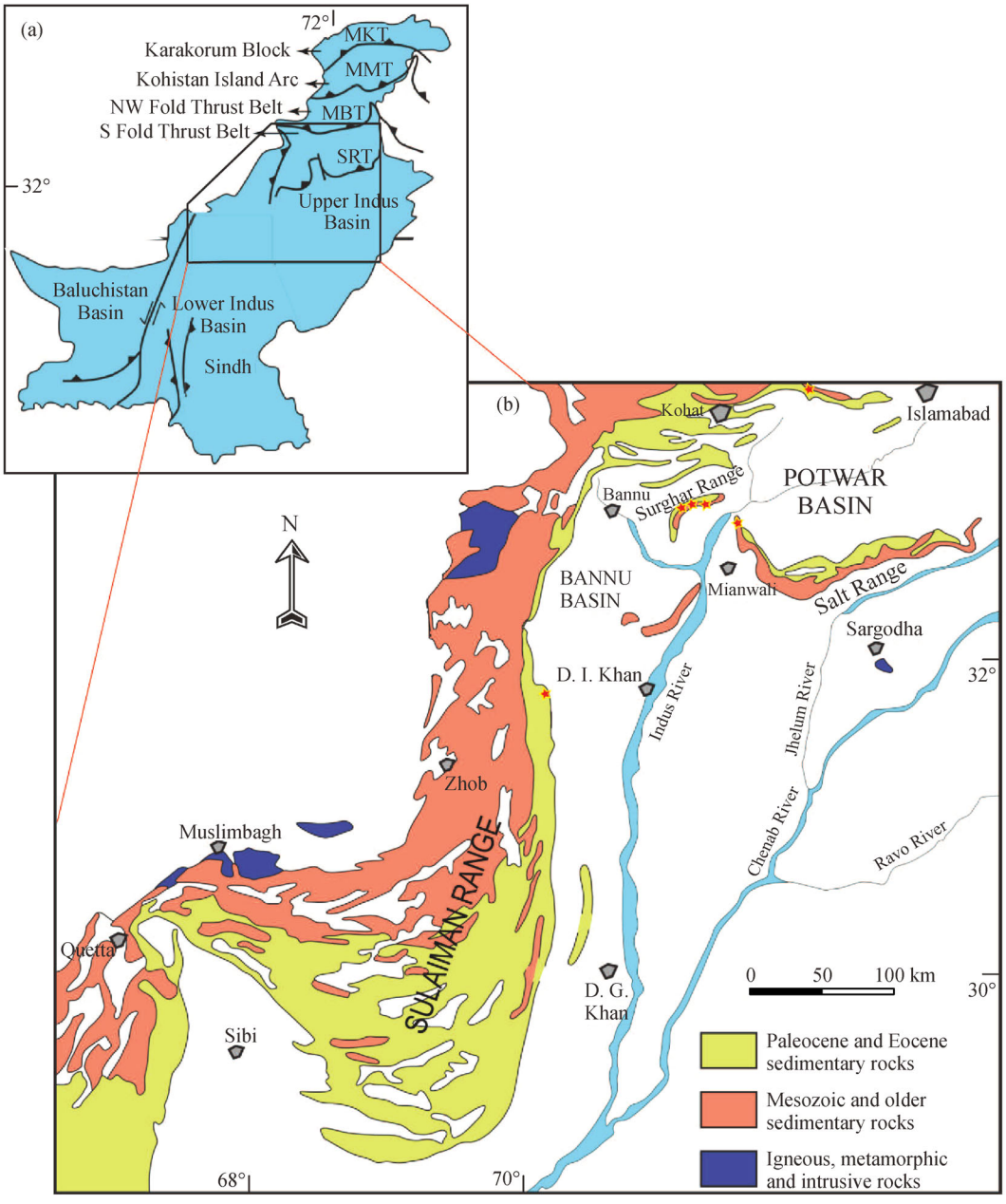

Fig. 2 The location of studied stratigraphic sections, such as ACL-N Khai, Baroch Nala, Gula Khel Nala, Chichali Nala, Nammal gorge, and Mughal Kot sections represented by red star respectively in Indus Basin, Pakistan (Kazmi and Rana, 1982). The boundary between the Upper and Lower Indus Basin is approximately lies at the latitude of 32° 00′ and longitude of 70°00′.

tectonic rifting of Pangaea leading to the separation of the Indian Plate from the Arabian and African plates may have also affected the paleoclimate during the Triassic–Jurassic interval. This tectonic rifting during the Jurassic caused the subsidence of the west and northwest areas of the Indus Basin, forming marine deltaic deposits, i.e., the Salt Range and Kohat–Potwar plateaus (Iqbal et al., 2019). At the time of the Early Jurassic (Hettangian to Toarcian), the shoreline of the paleo-Tethys trended approximately north–south with respect to the current configuration and was nearly parallel to the eastern flank of the Indus Basin, Pakistan (Shah, 2009). This basin was oriented east–west with respect to the present north of the Indus Basin. The shoreline was eastward while the basin was westward, where a very shallow marine depositional system existed, represented by western parts of the Kohat Plateau and Sulaiman Range. In the Early Jurassic, a north–south oriented (with respect to the present north) belt of marginal marine depositional settings existed with a deltaic setting in the north currently occupied by the Upper Indus Basin. Clastic supply to the basin in the west and southwest was minimal to none by Zao River into the Lower Indus Basin,

i.e., the Kohat Plateau and Sulaiman Range (Shah, 2009). Therefore, conditions in the Lower Indus Basin were more favorable for carbonate production than those in the Upper Indus Basin. This difference in the depositional systems mainly controlled by the tectonics led to differences in the thickness of the organic-rich shale, with the deposition of thick organic shale intervals in the Upper Indus Basin compared to those of the Lower Indus Basin.

3 Methods and materials

The well-preserved Jurassic exposures of the Datta and Shinawari formations from the Upper sub-Indus Basin and the Chiltan Formation from the Lower sub-Indus Basin were selected for the present study. The selected stratigraphic sections from the Upper sub-Indus Basin are ACL-N Kahi village (ACL-N) in the Kala Chitta Range, Baroch Nala (BN), Chichali Nala (CN), and Gulla Khel Nala (GK) in the Surghar Ranges, Nammal Gorge section (NG) in the Salt Ranges and from Lower sub-Indus Basin Mughal Kot section (MK) in the Sulaiman Ranges (Fig. 2). The unweathered outcrop shale samples were obtained from a depth of 15–20 cm by a hand-held auger for laboratory analysis. The thickness of the formations was measured with the help of a Jacob staff, and a high-magnification Nikon camera was used to capture the field photographs. The palynofacies and palynology slides were prepared from black shale samples according to the standard procedure defined in Wood et al. (1996). The slides were examined via transmitted light microscopy with three hundred counts following the procedure (Steffen and Gorin, 1993). The amorphous organic matter (AOM) and palynomorphs were analyzed under epifluorescence microscopy (EF), microscopy (Nikon SMZ-25), and polarizing microscopy (Nikon OS-F12), respectively.

For trace element analysis, all samples were crushed, pulverized, and dried in an oven at 105°C for 24 h. A 0.5 g sample was dissolved in 10 mL concentrated aqua regia, which was boiled in reflux for 3 h. Then the solution was cooled and filtered through No. 42 Whatman filter paper into a 50 mL volumetric flask. The trace element analysis was performed through inductively coupled plasma-optical emission spectrometry (ICP-OES), and a few samples were examined under inductively coupled plasma-mass spectrometry (ICP-MS). The instrumental and operating conditions of ICP-OES are as follows: The RF power value is 1150 W and the pump rate is 50 r/min. The auxiliary, nebulizer and coolant of gas flow rates are 0.5 L/min, 0.7 L/min, and 12 L/min, respectively. The normal purge gas flow, radial view mode plasma, aerosol carrier has argon gas, spectrometer flushing argon gas, and the sample uptake are 2.0 mL/min, and the integration time is 5.0 s (Naeem et al., 2011). A certified reference solution from Alfa Aesar was used for the calibration and correction factors of the ICP-OES instrument. The chosen analytical emission lines (nm) of trace elements (TM) are as follows: Aluminum (Al); Copper (Cu); Chromium (Cr); Magnesium (Mg); Manganese (Mn); Antimony (Sb); Molybdenum (Mo); Nickel (Ni); Thallium (Th); Titanium (Ti); Uranium (U); Cadmium (Cd); Vanadium (V) and Zinc (Zn). Furthermore, the stable carbon and oxygen isotopic analyses and total organic contents were analyzed using VG Isogas Prism III isotope ratio mass spectrometer with the elemental analyzer at the School of Geoscience, Wolfson Laboratory, Edinburgh, UK (UK), and Delta plus Advantage, Thermo-Fisher Scientific. The acetanilide and PACS-2 (National Research Council Canada) (Ali et al., 2018) $CaCO_3$ and V-PDB: Vienna-Pee Dee Belemnite standards were used for instrument calibration.

4 Results

4.1 Trace element analysis

The results of the trace elements of the Lower to Middle Jurassic shale from the Indus Basin are shown in Tables 1–4. The samples codes such as NS, ND, BS, BD, SS, CC, GS, GD, and NG belong to Upper Indus Basin, and MG belong to Lower Indus Basin, Pakistan. Among the 50-one studied samples, these redox elements (Table 1) are represented and discussed based on the ratio and individual behavior of V, Ni, Mo, Cu, and Cr. The detrital and paleo-anoxic settings are marked by Ti & Al and Mo, Zn, Ni, Cu, Cr, and V ratios, respectively. While the abundance of organic matter is determined to correlate the individual elements such as V, Ni, and Cu with total organic content (TOC). Additionally, the enrichment factor (EF) is used to accurately determine the paleo-environmental conditions. The EF was determined from the composition of post-Archean Australian shales (PAAS) following the methods described by noteworthy literature (Taylor and McLennan, 1985; Wedepohl, 1971, 1991; McLennan, 2001; Brumsack, 2006). The enriched elements are expressed by an EF greater than 1.0, whereas depleted elements have an EF less than 1.0. In the studied samples, the EF values of Al, Cu, Mn, Ni, Zn were less than 1.0, the EF values of Ti and V were equal to 1.0, and the EF values of Cr and Mo were greater than 1.0 and reached 3.0 (Table 2).

4.2 Geochemical and palynofacies analysis

Bulk carbon and oxygen isotopic study: The bulk carbon isotopic values obtained from the Lower Jurassic Datta Formation range from −2‰ to −3‰ in most of the studied samples, except for a single sample having no signal observed during laboratory analysis. Although in the Middle Jurassic Shinawari Formation, the $\delta^{13}C$ values of the organic matter show a negative excursion of 5‰–6‰

Table 1 The composition of trace elements (weight in grams) in the Lower to Middle Jurassic rocks of the Indus Basin

Sample No.	the composition of trace elements/($\mu g \cdot g^{-1}$)								
	Al	Cr	Cu	Mn	Mo	Ni	Ti	V	Zn
PAAS	84000.0	100.0	75.0	1400.0	1.0	60.0	3000.0	140.0	80.0
NS 10	11261.0	90.17	6.12	7.13	2.1	15.23	3000.35	130.21	8.35
NS 08	11855.2	80.17	8.02	11.13	3.53	21.17	3445.98	130.31	11.94
ND 25	11966.0	80.96	17.72	19.53	2.22	30.66	3499.11	137.17	29.11
ND 20	10967.1	132.1	33.52	15.45	2.56	17.16	3470.45	125.46	25.21
ND 15	10960.3	99.17	23.12	21.88	3.45	13.5	2976.33	155.98	25.54
ND 12	11905.8	82.16	18.22	16.4	3.56	13.65	2999.76	130.1	33.74
ND 06	12965.7	92.16	13.02	18.45	3.5	12.56	3300.23	127.67	30.24
ND 02	12967.7	73.17	12.02	17.03	5.57	44.77	3746.51	254.39	24.64
BS 11	13280.3	53.69	0	109.4	0	15.19	671.81	188.55	0
BS 09	13381.3	54.79	0	139.49	0	10.15	1950.85	145.34	3.65
BD 46	31500.4	71.12	6.9	189.32	3.21	13.53	1190.17	146.26	44.15
BD 36	30530.8	76.32	10.55	190.65	3.53	21.44	1011.99	136.44	51.33
BD 29	31531.5	70.11	7.7	187.41	2.57	13.95	1399.34	137.57	45.15
BD 21	31601.2	70.12	6.7	190.35	2.91	45.32	3500.17	146.23	38.61
BD 19	31501.4	71.32	6.8	188.31	0	13.33	2910.07	147.03	35.01
BD 15	31932.7	81.41	15.22	199.91	10.11	11.76	2980.64	135.55	31.15
BD 12	30112.1	65.44	5.11	185.46	4.3	12.86	2999.61	145.15	32.31
BD 06	31011.7	70.13	9.26	118.21	5.5	13.66	2975.94	139.95	33.55
SS 20	21211.5	77.59	16.52	35.43	0	7.66	4041.66	129.36	33.62
SS 21	73756.2	97.6	24.82	348.25	6.2	38.36	4016.75	132.14	217.95
SS 22	78344.1	142.05	8.21	213.37	44.7	141.93	4117.44	182.54	266.54
SS 23	29455.8	99.88	44.29	190.64	0	35.46	4423.04	187.44	43.82
SS 24	65633.5	86.41	44.2	295.7	3.1	41.45	4133.04	171.9	77.01
SS 25	66541.2	99.13	38.75	275.91	1.05	35.45	4099.04	165.98	99.91
CC 26	66633.5	97.41	33.24	272.96	3.11	38.4	3187.88	173.45	79.01
CC 27	63445.9	106.83	26.77	118.56	0	25.05	2389.78	175.95	44.95
CC 28	42777.7	96.1	24.34	888.13	3.2	43.14	1599.11	125.46	55.56
CC 29	39955.4	96.29	17.69	798.87	1.7	40.28	2767.11	122.57	55.47
CC 30	47177.4	86.26	27.12	265.27	0	30.75	1667.34	120.35	50.47
CC 31	55655.1	114.54	25.07	282.13	2.63	37.24	3746.51	206.3	69.74
GS 20	21211.5	76.59	15.52	34.43	0	7.36	4040.66	128.36	32.62
GS 12	73754.2	94.6	23.82	347.25	3.2	36.36	4006.75	172.14	207.95
GS 10	78334.1	132.05	9.21	203.37	34.7	152.93	4110.44	181.54	261.54
GS 09	29435.8	98.88	41.29	199.64	0	33.46	4403.04	187.44	42.82
GS 06	65623.5	85.41	41.2	285.7	2.1	40.45	4103.04	171.9	76.01
GS 05	66511.2	95.13	39.75	295.91	2.05	36.45	4093.04	165.98	98.91
GS 02	66623.5	90.41	31.24	282.96	2.11	37.4	3186.88	173.45	78.01
GD 20	63440.9	100.83	23.77	108.56	0	24.05	2380.78	175.95	43.95
GD 16	42775.7	99.1	21.34	878.13	2.2	42.14	1598.11	125.46	57.56
GD 12	39925.4	92.29	16.69	788.87	1.69	39.28	2733.11	122.57	53.47
GD 09	47117.4	80.26	26.12	255.27	0	29.75	1637.34	120.35	53.47
GD 01	55650.1	117.54	24.07	272.13	2.23	36.24	3746.51	206.3	69.74

(*Continued*)

Sample No.	the composition of trace elements/(μg·g^{-1})								
	Al	Cr	Cu	Mn	Mo	Ni	Ti	V	Zn
NG 19	42235.6	19.29	19.29	789.3	2.1	40.01	2245.41	119.95	52.74
NG 08	55622.1	23.08	23.08	277.23	2.5	35.42	3165.56	140.99	95.81
NG 04	59008.5	22.87	22.87	254.84	2.99	38.83	3085.71	172.03	98.88
NG 01	52496.0	35.66	35.66	246.91	3.3	42.24	3005.86	190.07	81.95
MS 17	21135.0	28.46	15.64	39.59	0.78	16.41	3212.05	60.93	21.9
MS 22	28557.5	29.22	4.65	87.63	2.67	0.71	2064.84	73.63	8.64
MS 29	45927.3	16.49	8.65	77.15	2.89	0.56	3042.69	48.88	12.03
MS 48	11107.0	89.35	9.75	115.7	0	1.91	2055.56	29.24	12.03
MS 53	9489.37	21.28	7.59	8.82	0	1.89	356.65	99.24	12.0

Table 2 The enrichment factor (EF) of trace elements in the Lower to Middle Jurassic rocks of the Indus Basin after normalized with PASS

Sample No.	EF of trace elements								
	Al	Cr	Cu	Mn	Mo	Ni	Ti	V	Zn
NS 10	0.13	0.90	0.08	0.01	2.10	0.25	1.00	0.93	0.10
NS 08	0.14	0.80	0.11	0.01	3.53	0.35	1.15	0.93	0.15
ND 25	0.14	0.81	0.24	0.01	2.22	0.51	1.17	0.98	0.36
ND 20	0.13	1.32	0.45	0.01	2.56	0.29	1.16	0.90	0.32
ND 15	0.13	0.99	0.31	0.02	3.45	0.23	0.99	1.11	0.32
ND 12	0.14	0.82	0.24	0.01	3.56	0.23	1.00	0.93	0.42
ND 06	0.15	0.92	0.17	0.01	3.50	0.21	1.10	0.91	0.38
ND 02	0.15	0.73	0.16	0.01	5.57	0.75	1.25	1.82	0.31
Ave. EF	0.14	0.91	0.22	0.01	3.31	0.35	1.10	1.06	0.29
BS 11	0.16	0.54	0.00	0.08	0.00	0.25	0.22	1.35	0.00
BS 09	0.16	0.55	0.00	0.10	0.00	0.17	0.65	0.38	0.05
BD 46	0.38	0.71	0.09	0.14	3.21	0.23	0.40	0.71	0.55
BD 36	0.36	0.76	0.14	0.14	3.53	0.36	0.34	0.74	0.64
BD 29	0.38	0.70	0.10	0.13	2.57	0.23	0.47	0.98	0.56
BD 21	0.38	0.70	0.09	0.14	2.91	0.76	1.17	1.04	0.48
BD 19	0.38	0.71	0.09	0.13	0.00	0.22	0.97	1.05	0.44
BD 15	0.38	0.81	0.20	0.14	10.11	0.20	0.99	0.97	0.39
BD 12	0.36	0.65	0.07	0.13	4.30	0.21	1.00	1.04	0.40
BD 06	0.37	0.70	0.12	0.08	5.50	0.23	0.99	1.00	0.42
Ave. EF	0.33	0.68	0.09	0.12	3.21	0.29	0.72	1.05	0.39
SS 20	0.25	0.78	0.22	0.03	0.00	0.13	1.35	0.92	0.42
SS 21	0.88	0.98	0.33	0.25	6.20	0.64	1.34	0.94	2.72
SS 22	0.93	1.42	0.11	0.15	44.70	0.37	1.37	0.86	3.33
SS 23	0.35	1.00	0.59	0.14	0.00	0.59	1.47	1.34	0.55
SS 24	0.78	0.86	0.59	0.21	3.10	0.69	1.38	1.23	0.96
SS 25	0.79	0.99	0.52	0.20	1.05	0.59	1.37	1.19	1.25
CC 26	0.79	0.97	0.44	0.19	3.11	0.64	1.06	1.24	0.99
CC 27	0.76	1.07	0.36	0.08	0.00	0.42	0.80	1.26	0.56
CC 28	0.51	0.96	0.32	0.63	3.20	0.72	0.53	0.90	0.69
CC 29	0.48	0.96	0.24	0.57	1.70	0.67	0.92	0.88	0.69

(*Continued*)

Sample No.	EF of trace elements								
	Al	Cr	Cu	Mn	Mo	Ni	Ti	V	Zn
CC 30	0.56	0.86	0.36	0.19	0.00	0.51	0.56	0.86	0.63
CC 31	0.66	1.15	0.33	0.20	2.63	0.62	1.25	1.47	0.87
Ave. EF	0.65	1.00	0.37	0.24	5.47	0.72	1.12	1.13	1.14
GS 20	0.25	0.77	0.21	0.02	0.00	0.12	1.35	0.92	0.41
GS 12	0.88	0.95	0.32	0.25	3.20	0.61	1.34	0.23	2.60
GS 10	0.93	1.32	0.12	0.15	34.70	2.55	1.37	1.30	3.27
GS 09	0.35	0.99	0.55	0.14	0.00	0.56	1.47	0.34	0.54
GS 06	0.78	0.85	0.55	0.20	2.10	0.67	1.37	1.23	0.95
GS 05	0.79	0.95	0.53	0.21	2.05	0.61	1.36	1.19	1.24
GS 02	0.79	0.90	0.42	0.20	2.11	0.62	1.06	0.24	0.98
GD 20	0.76	1.01	0.32	0.08	0.00	0.40	0.79	1.26	0.55
GD 16	0.51	0.99	0.28	0.63	2.20	0.70	0.53	0.90	0.72
GD 12	0.48	0.92	0.22	0.56	1.69	0.65	0.91	0.88	0.67
GD 09	0.56	0.80	0.35	0.18	0.00	0.50	0.55	0.86	0.67
GD 01	0.66	1.18	0.32	0.19	2.23	0.60	1.25	0.86	0.87
Ave. EF	0.65	0.97	0.35	0.24	4.19	0.72	1.11	1.15	1.12
NG 19	0.50	0.99	0.26	0.56	2.10	0.67	0.75	0.86	0.66
NG 08	0.66	0.97	0.31	0.20	2.50	0.59	1.06	1.01	1.20
NG 04	0.70	0.94	0.30	0.18	2.99	0.65	1.03	1.23	1.24
NG 01	0.62	1.06	0.48	0.18	3.30	0.70	1.00	1.36	1.02
Ave. EF	0.62	0.99	0.34	0.28	2.72	0.65	0.96	1.11	1.03
MS 17	0.25	0.28	0.21	0.03	0.78	0.27	1.07	0.44	0.27
MS 22	0.34	0.29	0.06	0.06	2.67	0.01	0.69	0.53	0.11
MS 29	0.55	0.16	0.12	0.06	2.89	0.01	1.01	0.35	0.15
MS 48	0.13	0.89	0.13	0.08	0.00	0.03	0.69	0.21	0.15
MS 53	0.11	0.21	0.10	0.01	0.00	0.03	0.12	0.71	0.15
Ave. EF	0.28	0.37	0.12	0.05	1.27	0.07	0.72	0.45	0.17

per mil shift (−24‰ to −28‰) in the Chichali Nala (Ali et al., 2018), the −5‰ to −9‰ negative $\delta^{13}C$ excursion and one positive value had been recorded from the rest of the studied sections in the Indus Basin.

Organic geochemical analysis: The major values of TOC are 0.11% to 4.51% in the studied sections of the Indus Basin, Pakistan. TOC values ≥ 2% are categorized as high-potential source rock, and those ⩽2% are known as non-high potential source rock (Table 3).

Palynofacies analysis: The Lower Jurassic Datta Formation palynofacies (DFPF) are subdivided into types of A, B, and C. The petrographic constituents of DFPF-A are composed of phytoclasts (68% to 79% with an average of 74%) (More than 10% is opaque), palynomorphs (10% to 24% with an average of 18%), and amorphous organic matter (AOM) (3% to 12% with an average of 6%). The phytoclasts are reddish-brown and black, with less internal structure, having various shapes such as elongated, circular/spherical, and blade. The color ranges of AOM are yellowish-brown, while the documented lowest fraction of tracheids and cuticles are well preserved internal structures (Figs. 3(a)–3(c)). The palynofacies DFPF-B are composed of phytoclasts (62%), amorphous organic matter (AOM) (20%), and palynomorphs (18%). The characteristics of phytoclasts are similar to the previous palynofacies (Fig. 3(f)), and the palynofacies DFPF-C are comprised of phytoclasts (85%–89%), palynomorphs (5%–10%), and amorphous organic matter (AOM) (4%–6%). The properties of phytoclasts are similar to the previous palynofacies (Fig. 3(g)). The Middle Jurassic Shinawari Formation and Chiltan Limestone palynofacies (SFPF) are represented by SFPF A and B. SFPF A is composed dominantly of phytoclasts (85%–86%), palynomorphs (10%), and amorphous organic matter (AOM) (5%), while SFPF B is represented by phytoclasts (57%), palynomorphs (33%), and AOM (10%). These palynofa-

cies SFPF A and B are used after the studies of Ali et al. (2019). The Middle Jurassic Chiltan Limestone has SFPF B palynofacies composed of phytoclasts (62%), palynomorphs (29%), and AOM (9%) (Fig. 3(h)).

5 Discussion

5.1 Variation of detrital flux concentration

The elemental ratios such as Ti/Al and Si/Al are considered to be the key proxies that are used to define the detrital input concentration into the basin (Werne et al., 2002; Sageman et al., 2003; Rimmer et al., 2004; Li et al., 2015). In the present study, six different stratigraphic sections of the Indus Basin show no uniform distribution of Ti/Al, and most of the samples are recorded with low values of this ratio (1.96 on average). This suggests heterogeneous sources and variation in the amount of the detrital supply. Generally, Ti has been shown to be abundant in association with certain accessory minerals present in sediments. And it is present in the coarse-grain portion of fine-texture siliciclastic sediments (Brumsack, 1986; Calvert and Pedersen, 2007; Zheng et al., 2019). According to Rachold

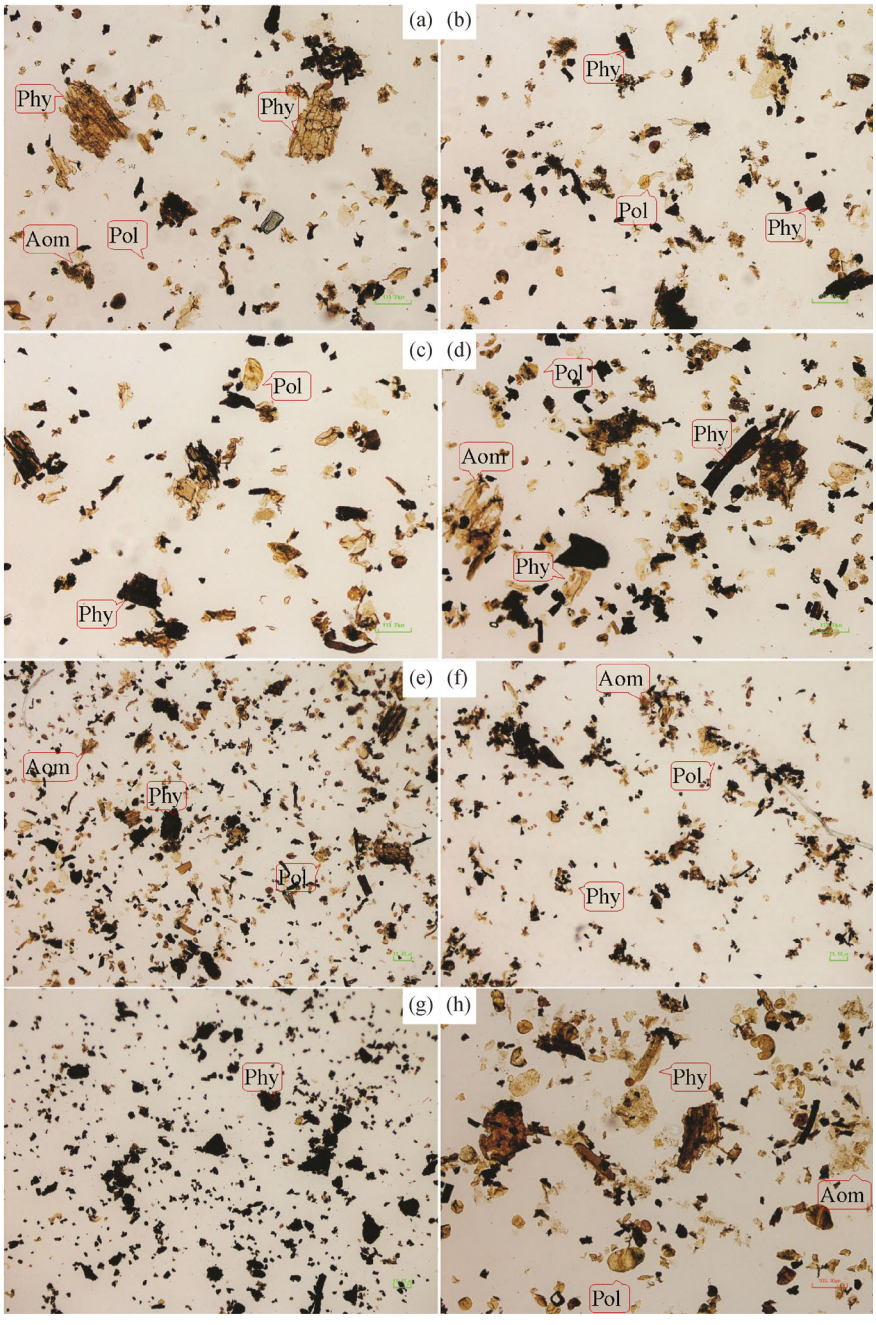

Fig. 3 Shale palynofacies of the Indus Basin, Pakistan. (a)–(e) DFPF-A; (f) DFPF-B; (g) DFPF-C; (h) Chiltan Limestone SFPF B.

and Brumsack (2001), Ti is considered as an indicator of aeolian detrital supply. The lower Ti/Al ratios reflect an enhanced Ti-depleted fluvial contribution (Scopelliti et al., 2004). The values of Cr and Ti/Al are used to define the detrital influx into the basin (Soua, 2011), which indicates a low amount of clastic input with low oxygen supply in the studied formations of the Indus Basin. Furthermore, the Ti/Al elemental ratio is not consistent with organic matter enrichment, i.e., low values of the Ti/Al ratio does not indicate organic-rich intervals and vice versa. Therefore, the current work suggests that the extra aeolian source of Ti is the main factor of this inconsistency and that more than one single source is involved in detrital input (Figs. 4–5 and Table 3).

Table 3 The ratios of various elements from normalized data used for depositional environment interpretation in the studied sections

Sample No.	the ratios of various elements											TOC/%
	V/Cr	V/Mo	V/Ni	V/(V + Ni)	V/(V + Cr)	Ti/Al	Cu/Al	Ni/Al	Mo/Al	Cr/Al	(Cu + Mo)/Zn	
NS 10	1.03	0.44	3.66	0.79	0.51	7.46	0.61	1.89	15.66	6.73	20.90	0.11
NS 08	1.16	0.26	2.64	0.73	0.54	8.14	0.76	2.50	25.01	5.68	24.37	0.13
ND 25	1.21	0.44	1.92	0.66	0.55	8.19	1.66	3.59	15.58	5.68	6.75	0.15
ND 20	0.68	0.35	3.13	0.76	0.40	8.86	3.42	2.19	19.61	10.12	9.54	1.55
ND 15	1.12	0.32	4.95	0.83	0.53	7.60	2.36	1.72	26.44	7.60	11.77	4.15
ND 12	1.13	0.26	4.08	0.80	0.53	7.05	1.71	1.61	25.12	5.80	9.02	4.09
ND 06	0.99	0.26	4.36	0.81	0.50	7.13	1.12	1.36	22.68	5.97	9.72	4.22
ND 02	2.48	0.33	2.44	0.71	0.71	8.09	1.04	4.83	36.08	4.74	18.60	4.21
BS 11	2.51	0.00	5.32	0.84	0.71	1.42	0.00	1.60	0.00	3.40	0.00	1.37
BS 09	1.89	0.00	2.25	0.69	0.41	4.08	0.00	1.06	0.00	3.44	0.00	0.51
BD 46	1.47	0.22	3.17	0.76	0.50	1.06	0.25	0.60	8.56	1.90	5.98	0.71
BD 36	1.28	0.21	2.08	0.68	0.49	0.93	0.39	0.98	9.71	2.10	5.72	0.41
BD 29	1.40	0.38	4.23	0.81	0.58	1.24	0.27	0.62	6.85	1.87	4.74	1.23
BD 21	1.49	0.36	1.38	0.58	0.60	3.10	0.24	2.01	7.74	1.86	6.21	2.15
BD 19	1.47	0.00	4.73	0.83	0.60	2.59	0.24	0.59	0.00	1.90	0.21	2.4
BD 15	1.19	0.10	4.94	0.83	0.54	2.61	0.53	0.52	26.59	2.14	26.49	0.17
BD 12	1.58	0.24	4.84	0.83	0.61	2.79	0.19	0.60	12.00	1.83	10.82	0.58
BD 06	1.43	0.18	4.39	0.81	0.59	2.69	0.33	0.62	14.90	1.90	13.41	1.62
SS 20	1.19	0.00	7.24	0.88	0.54	5.34	0.87	0.51	0.00	3.07	0.52	0.5
SS 21	0.97	0.15	1.48	0.60	0.49	1.52	0.38	0.73	7.06	1.11	2.40	0.5
SS 22	0.92	0.02	2.35	0.70	0.38	1.47	0.12	2.54	47.93	1.52	13.45	0.5
SS 23	1.34	0.00	2.27	0.69	0.57	4.20	1.68	1.69	0.00	2.85	1.08	0.8
SS 24	1.42	0.40	1.78	0.64	0.59	1.76	0.75	0.88	3.97	1.11	3.83	1.5
SS 25	1.20	1.13	2.01	0.67	0.54	1.72	0.65	0.75	1.33	1.25	1.25	0.5
CC 26	1.27	0.40	1.94	0.66	0.56	1.34	0.56	0.81	3.92	1.23	3.60	1.3
CC 27	1.18	0.00	3.01	0.75	0.54	1.05	0.47	0.55	0.00	1.41	0.64	2.34
CC 28	0.93	0.28	1.25	0.55	0.48	1.05	0.64	1.41	6.28	1.89	5.07	1.86
CC 29	0.91	0.52	1.30	0.57	0.48	1.94	0.50	1.41	3.57	2.02	2.79	2.3
CC 30	1.00	0.00	1.68	0.63	0.50	0.99	0.64	0.91	0.00	1.54	0.57	0.95
CC 31	1.29	0.56	2.37	0.70	0.56	1.88	0.50	0.94	3.97	1.73	3.40	2.4
GS 20	1.20	0.00	7.47	0.88	0.54	5.33	0.82	0.49	0.00	3.03	0.51	0.62
GS 12	1.30	0.07	0.38	0.27	0.20	1.52	0.36	0.69	3.64	1.08	1.35	0.61
GS 10	0.98	0.04	0.51	0.34	0.50	1.47	0.13	2.73	37.21	1.42	10.65	1.06
GS 09	1.35	0.00	0.61	0.38	0.26	4.19	1.57	1.59	0.00	2.82	1.03	0.78
GS 06	1.44	0.58	1.82	0.65	0.59	1.75	0.70	0.86	2.69	1.09	2.79	2.09
GS 05	1.25	0.58	1.95	0.66	0.55	1.72	0.67	0.77	2.59	1.20	2.09	1.07
GS 02	1.37	0.11	0.38	0.28	0.21	1.34	0.53	0.79	2.66	1.14	2.59	0.98

(*Continued*)

Sample No.	the ratios of various elements											TOC/%
	V/Cr	V/Mo	V/Ni	V/(V + Ni)	V/(V + Cr)	Ti/Al	Cu/Al	Ni/Al	Mo/Al	Cr/Al	(Cu + Mo)/Zn	
GD 20	1.25	0.00	3.14	0.76	0.55	1.05	0.42	0.53	0.00	1.34	0.58	2.19
GD 16	0.90	0.41	1.28	0.56	0.47	1.05	0.56	1.38	4.32	1.95	3.45	1.73
GD 12	0.95	0.52	1.34	0.57	0.49	1.92	0.47	1.38	3.56	1.94	2.86	1.85
GD 09	1.07	0.00	1.73	0.63	0.52	0.97	0.62	0.88	0.00	1.43	0.52	0.82
GD 01	1.25	0.38	1.42	0.59	0.42	1.89	0.48	0.91	3.37	1.77	2.93	0.89
NG 19	0.86	0.41	1.28	0.56	0.46	1.49	0.51	1.33	4.18	1.98	3.58	0.51
NG 08	1.04	0.40	1.71	0.63	0.51	1.59	0.46	0.89	3.78	1.46	2.34	4.51
NG 04	1.31	0.41	1.90	0.66	0.57	1.46	0.43	0.92	4.26	1.33	2.67	3.76
NG 01	1.29	0.41	1.93	0.66	0.56	1.60	0.76	1.13	5.28	1.69	3.69	0.92
MS 17	1.53	0.56	1.59	0.61	0.60	4.26	0.83	1.09	3.10	1.13	3.61	0.76
MS 22	1.80	0.20	44.44	0.98	0.64	2.02	0.18	0.03	7.85	0.86	25.30	2. 08
MS 29	2.12	0.12	37.41	0.97	0.68	1.86	0.21	0.02	5.29	0.30	19.99	2. 15
MS 48	0.23	0.00	6.56	0.87	0.19	5.18	0.98	0.24	0.00	6.76	0.86	1. 50
MS 53	3.33	0.00	22.50	0.96	0.77	1.05	0.90	0.28	0.00	1.88	0.67	2. 81

5.2 Paleo redox condition

Element enrichment: The variation and wide range presence of redox-sensitive elements (Ni, V, Mo, Mn, U, Cu, Cr, Re, Cd, Sb, and Ti) in sediments reflect the ancient oceanographic setting (Brumsack, 2006; Tribovillard et al., 2006; Chen et al., 2013; Pi et al., 2014; Baioumy and Lehmann, 2017). These elements are significantly enriched in reducing anoxic depositional sediments. The enrichment in the concentration of these elements in the current studied Jurassic black shale is strong evidence of anoxic conditions (Pi et al., 2014). In the current study, the formations are enriched in Cr and Mo, slightly enriched in Ti and V, and drained of Al, Cu, Mn, Ni, and Zn. The enrichment of Mo and V in the shales of the Lower to Middle Jurassic indicates that the deposition had taken place in oxygen-depleted water under anoxic conditions. The absence of U shows that the bacterial sulfate reduction did not take place throughout the time of deposition (Tribovillard et al., 2006; Soua, 2011). Basically, the V and Mo enrichment and the absence of U indicated suboxic/anoxic deposition with free hydrogen sulfide (Tribovillard et al., 2006). The anoxia of bottom water in ancient sediments has been determined from Mo enrichment when the other enriched redox-sensitive trace elements (i.e., Re and U) are absent, although the Mo enrichment may be due to boidal pyrite in the process of early diagenesis (Tribovillard et al., 2008). In the studied strata, boidal pyrite is absent or rarely present, so the enriched value of Mo is depositional and valid in this study. According to McManus et al. (2006) and Zheng et al. (2000), Mo accumulation occurred under less anoxic conditions. Thus, bottom waters were in less-reducing dysoxic to anoxic conditions (Figs. 4–5 and Table 2).

Bottom water oxygenation conditions: for reliable interpretation, different ratios of trace elements are used and the individual values of various elements are not used to interpret the geological process (Hatch and Leventhal, 1992; Jones and Manning, 1994). The V/(V + Ni) value is 0.75, and the V/(V + Cr) value is 0.60 in the studied strata, supporting the anoxic/reduced state of the depositional setting (Hatch and Leventhal, 1992; Jones and Manning, 1994; Rimmer, 2004; Baioumy and Lehmann, 2017). Thus, variations in the V/(V + Ni) and V/(V + Cr) ratios could indicate relative changes in oxygenation, with higher ratios signaling more strongly anoxic conditions of deposition. The V/Cr ratio in the studied formations is 1.22, which falls in the oxic zone, supporting the Jones and Manning (1994) suggestion in the previous literature. The average value of V/Ni proxies in the Jurassic black shales is more than 3, indicating that deposition has taken place in a reducing setting and that the origin of these organic matters is terrestrial to marine in nature (Galarraga et al., 2008). The V/Mo ratios range from 0.18 to 0.30, the Mo/Al ratios range from 9.47 to 3.25, and the Cr/Al ratios range from 2.67 to 2.19, which indicates that the deposition of sediments occurred in depositional conditions with depleted oxygen, such as dysoxic to anoxic settings (Jones and Manning, 1994; Gallego-Torres et al., 2010; Li et al., 2015). Furthermore, the level of bottom water oxygenation is indicated by the (Cu + Mo)/Zn relationship, in which copper behaves partly as a micro-nutrient (Hallberg, 1982; Calvert and Pedersen, 1993; Szczepanik et al., 2010). The values of this proxy are enhanced under the prevailing reducing or anoxic conditions and decrease vice versa, i.e., the anoxic condition values documented for the Baltic Sea that range from 0.1 to 6 (Hallberg, 1982). The average (Cu + Mo)/Zn ratios for the samples from the

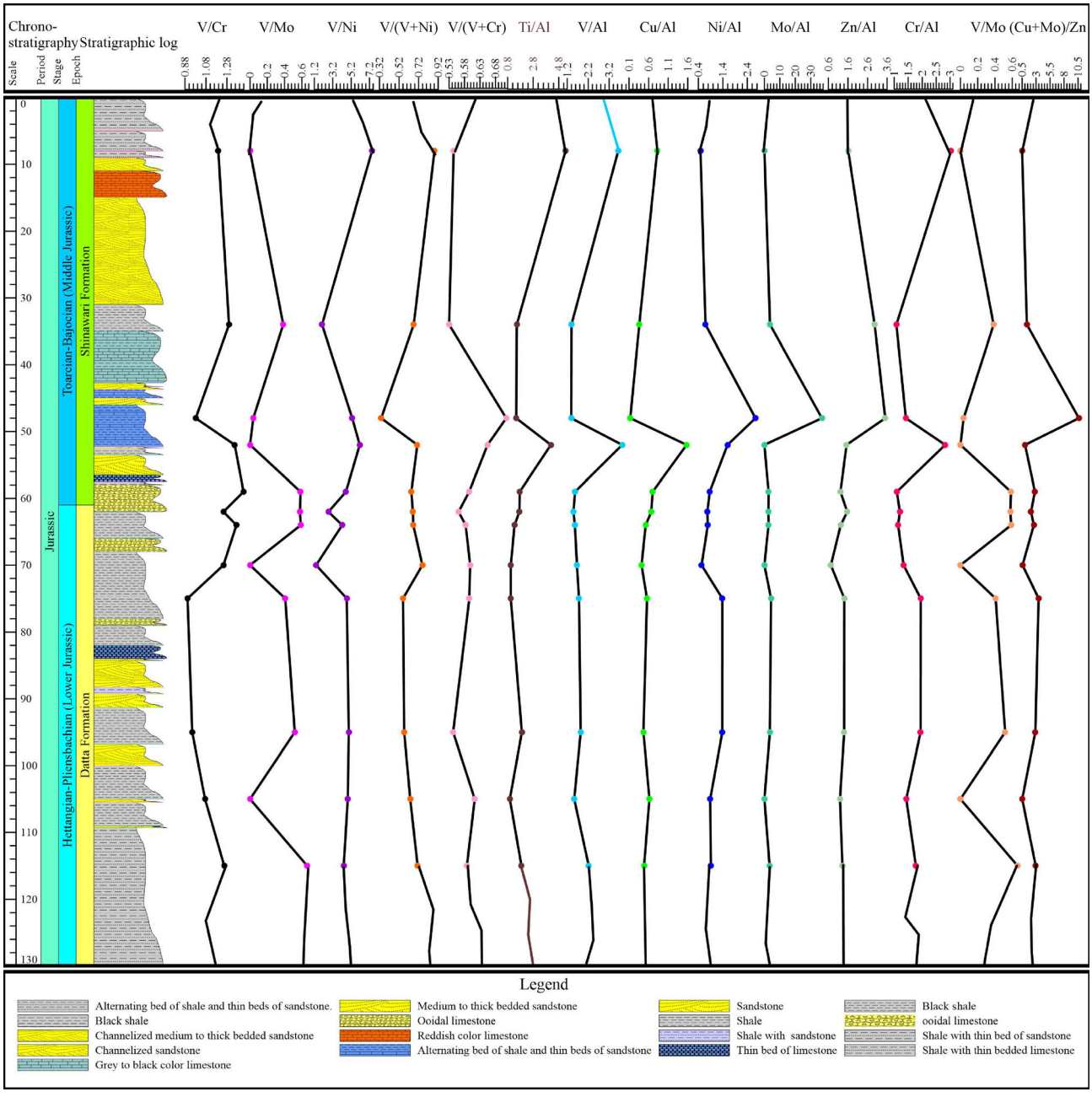

Fig. 4 The vertical distribution of various normalized trace elements concentrations across the Lower to Middle Jurassic strata, i.e., the Datta and Shinawari formations in the Upper Indus Basin, Pakistan.

Upper and Lower Indus Basin are 6.01 and 10.09, respectively, suggesting less-oxygenated anoxic bottom water conditions (Table 3).

Post-depositional reoxygenation: during the process of diagenesis, it is possible to develop reducing conditions by irreversible oxidation reactions in the sediments. These can restore the oxidation state after reduction in the deposited sediments, which can be related to glacial-interglacial transitions and turbidity deposits (Lyons et al., 2003; McManus et al., 2006). Specifically, the oxygen replenishment leads to U remobilization if oxygen enters the area where U has mainly precipitated as authigenic components. V, Cd, and Mo are less affected than U due to secondary reoxidation replenishment. Therefore, the absence of U in the studied Lower to Middle Jurassic rocks is either due to the post-depositional process or due to the absence of sulfate-reducing bacteria.

Role of anoxia: the anoxic events in Jurassic rocks featured the extensive development of euxinic and anoxic settings with subsequent deposition of organic dark black shales across the continents (Jenkyns, 2010). The exposed Lower Jurassic strata in our study area are composed of

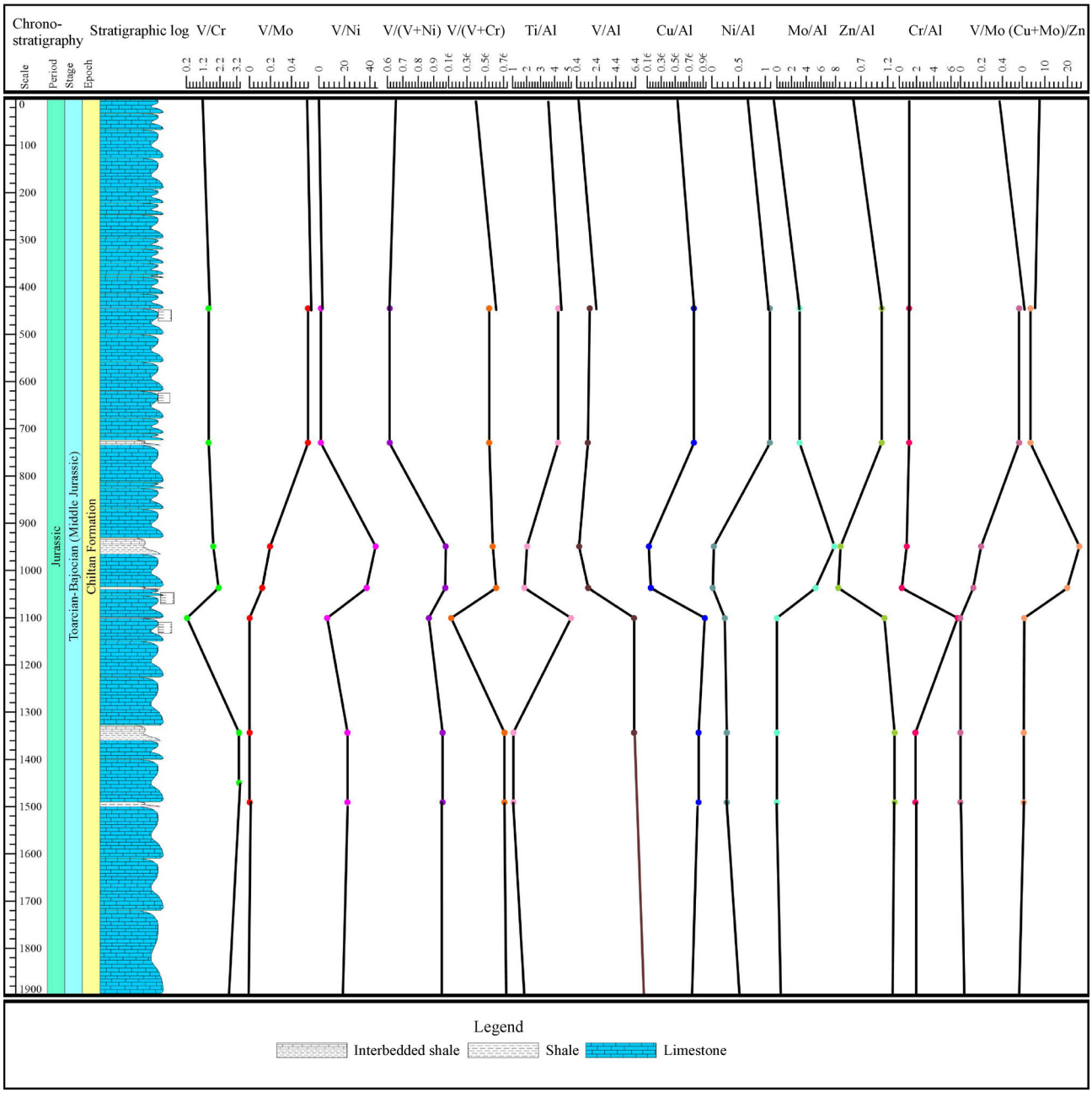

Fig. 5 The vertical distribution of various elemental ratio of Middle Jurassic (Toarcian-Bajocian) developed in the Chiltan Formation, Lower Indus Basin, Pakistan.

sandstone, shale, and subordinate limestone, while the Middle Jurassic strata represent shale, limestone, and subordinate sandstone units. The units are in the form of varied multifold cycles between carbonates and shale, which are the byproducts of the Neotethys Tectonics (Fürsich et al., 1992). The studied strata show high values of 5‰–6‰ per mil that shift from −24‰ to −28‰, suggesting a pronounced anoxic event and anoxia in the Lower to Middle Jurassic Indus Basin. The positive excursion values are reported from the gray shale in the study area, reflecting that anoxia is a significant factor in the formation of the black shale rocks.

Mineral phase: the coefficients of determination (r^2) between Mo and V, Zn, Cu, Cr, and Ni in the studied strata show positive correlations (Table 4). From the positive correlation between Mo and V, anoxic conditions are interpreted and occur in the common mineral phase (Yang et al., 2004), and the absence of any correlation portrays different mineral phases (Baioumy and Lehmann, 2017). To investigate the mode of occurrence or probable mineral

composition of the redox elements in Jurassic strata, the correlation between sensitive elements and main rock components must be investigated. The main rock components in the black shale are total organic content (TOC), Al and Ti detrital fractions. A slightly inconsistent correlation pattern between the sensitive elements and source rock constituents has occurred. In some stratigraphic sections, there is a positive correlation and vice versa. However, in the current study, we interpreted it as the mono-bi mineral phase under the redox condition of deposition (Table 4).

Tracers for organic matter abundance and input: different trace elements have different relationships with TOC despite differing redox conditions. For example, in contrast to U and V, Ni and Cu are mainly carried to the sediments fully allied with organic matter, forming an organometallic complex (Tribovillard et al., 2006). Subsequently, Ni and Cu can express the original occurrence of organic matter even if it partially disappeared after deposition. In this manner, Cu and Ni are better proxies for the organic matter richness than P and Ba (Tribovillard et al., 2006). From numerous investigations of sedimentary rocks (Tribovillard et al., 1994; Riboulleau et al., 2003; Algeo and Maynard, 2004; Tribovillard et al., 2006), it has been observed that U, V, Ni, and Cu-TOC covariation patterns depend upon the nature of open and closed marine systems. A classic example of open marine systems is that in which the dissolved trace element repository of ocean water is not depleted through the process of sedimentation. In restricted basins, the flux of trace elements can be exceeded compared to the source. Therefore, an association between TOC and trace elements seems unlikely in the current study or previous research (Algeo, 2004; Algeo and Maynard, 2004; Tribovillard et al., 2006). The positive and negative correlations of the Ni/Al and Cu/Al ratios with organic matter does not verify this clearly, but from the palynofacies investigation, it is clear that the deposition of sedimentary rocks of the Lower to Middle Jurassic of the Indus Basin took place in the episodes with a better influx of organic matter having mixed marine and clastic inputs (Table 4).

5.3 Depositional setting of black shale

The AOM-Phytoclast-Palynomorph ternary diagram of Tyson (1995) plots DFPF-A palynofacies corresponding to the Type II field, which represents the marginal dysoxic-anoxic basinal setting. DFPF-B palynofacies corresponds to the Type III field that represents a heterolithic, proximal shelf. DFPF-C palynofacies corresponds to the Type I field that is useful for representing a highly proximal shallow marine shelf depositional setting. In the Shinawari Formation and Chiltan Limestone, the AOM-Phytoclast-Palynomorph ternary diagram of Tyson (1995) plots SFPF A and B palynofacies in the Type II and Type III fields

Table 4 Spearman rank order correlations of the stratigraphic sections

GK	Al	Cr	Cu	Mn	Mo	Ni	Ti	V	Zn	TOC
Al	1.00									
Cr	–0.24	1.00								
Cu	0.46	–0.34	1.00							
Mn	0.48	0.01	0.25	1.00						
Mo	0.77	–0.12	–0.09	–0.10	1.00					
Ni	0.77	0.79	0.20	0.02	0.98	1.00				
Ti	0.77	0.79	0.37	–0.50	0.26	0.20	1.00			
V	0.77	0.79	0.30	–0.47	0.25	0.27	0.61	1.00		
Zn	0.77	0.79	0.29	–0.08	0.81	0.79	0.37	0.34	1.00	
TOC	0.14	0.01	0.06	0.39	–0.09	–0.01	–0.39	–0.12	–0.26	1.00
MK	Al	Cr	Cu	Mn	Mo	Ni	Ti	V	Zn	TOC
Al	1.00									
Cr	–0.24	1.00								
Cu	0.46	0.10	1.00							
Mn	0.48	0.67	0.25	1.00						
Mo	0.77	–0.12	–0.09	0.30	1.00					
Ni	0.77	0.79	0.20	–0.37	–0.28	1.00				
Ti	0.77	0.79	0.37	0.41	0.50	0.47	1.00			
V	0.77	0.79	0.30	–0.82	–0.07	–0.02	–0.65	1.00		
Zn	0.77	0.79	0.29	–0.39	–0.33	0.97	0.48	–0.10	1.00	
TOC	0.90	–0.49	–0.03	0.08	0.69	–0.21	0.50	–0.23	–0.06	1.00

correspond to a marginal dysoxic-anoxic basinal and proximal shelf setting, respectively (Fig. 6).

5.4 Depositional model and controlling factor of high-potential source rocks

What could be the possible driving mechanism for the deposition of local, regional, or global black shale occurrences during the Lower to Middle Jurassic? This question has long been debated and is still open. The Lower to Middle Jurassic shales are reported from the Eastern Tethys (Qiang et al., 2002; Yang et al., 2003; Chen et al., 2013; Srivastave and Ranawat, 2015; Ali et al., 2018; Ali et al., 2019), Central Tethys (Moshrif, 1987; Rousseau et al., 2005; Abdula et al., 2015), and Western Tethys (Nielsen et al., 2003; Løseth et al., 2009) with current study in the Indus Basin, Pakistan, but depositional setting debates still await further research and interpretation.

The geologic aspects that controlled the deposition of organic-rich dark shale also have been under consideration and debate for a long time. Therefore, an integrated approach is undertaken to assess the question of which factors are related to the depositional setting. The palynofacies analysis, organic geochemistry, carbon and oxygen isotope analysis, and trace element analysis provide important and noteworthy implications for the formation of organic-rich dark-gray shale. The controlling factors are high preservation, pronounced anoxia, low clastic dilution with enhanced particulate sedimentary particle supply, and deposition under favorable anoxic conditions. The palynofacies analysis shows that the deposition took place under extremely anoxic conditions proximal to the distal shelf setting. In addition to the palynofacies, different elemental ratios, such as Ti/Al and Cr, indicate a low detrital supply and low oxygen levels in more stratified and stagnant water. While the V/(V + Cr), V/(V + Ni), V/Mo, and V/Ni elemental ratios indicate anoxic conditions despite the V/Cr ratio showing oxic conditions. The Cu/Al, Ni/Al, Mo/Al and (Cu + Mo)/Zn elemental ratios are supported by oxygen-depleted sediments and the less-oxygenated conditions of bottom water with an influx of organic matter. The carbon and oxygen isotopic signals are fully supportive of anoxic events in water, which in the interim helped with the preservation of organic matter in shale. The studied sections show healthy values of carbon isotopes and the presence of Pliensbachian-Toarcian events in the studied strata. Globally, the strata related to anoxia show good source rocks. Therefore, the Jurassic shale in the Indus Basin is the collective result of the different processes responsible for the creation of anoxic conditions in water with the availability of the clastic and *in situ* nutrient supplies and their subsequent high preservation and deposition. In the published literature, it is ascertained that these three important factors

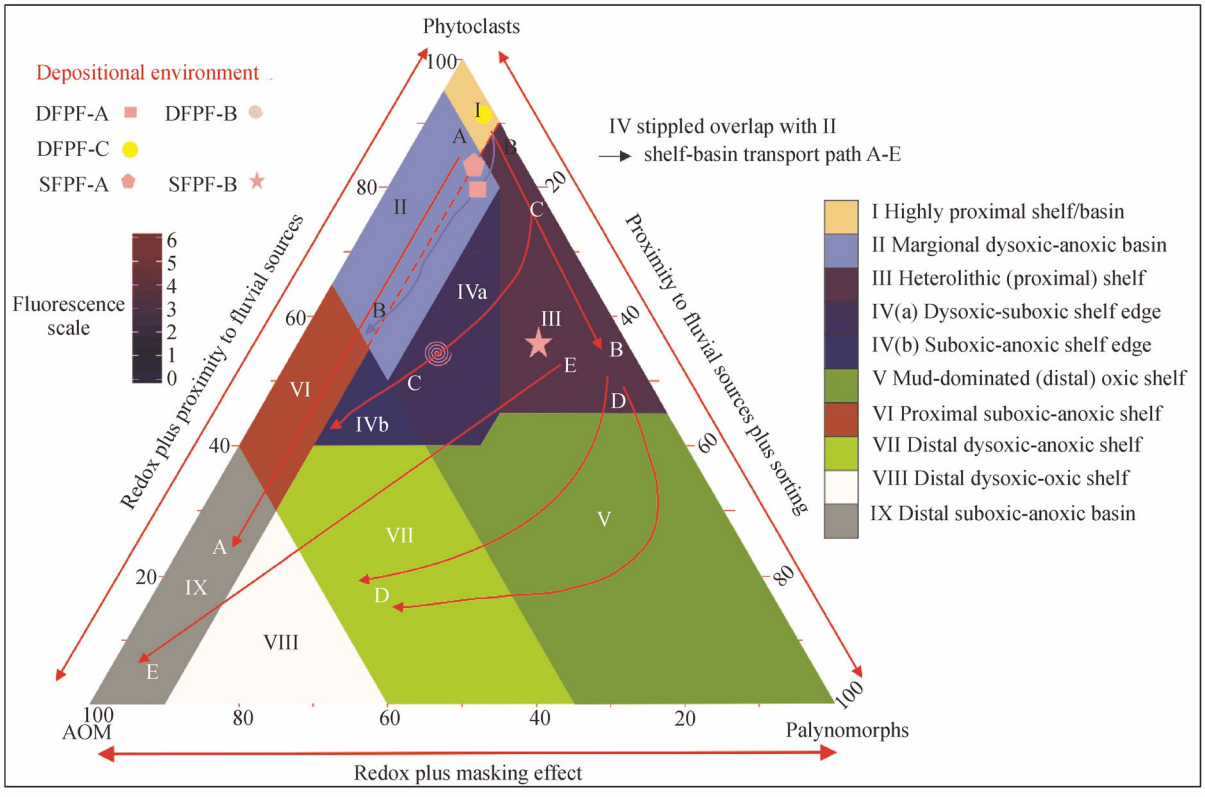

Fig. 6 Ternary AOM-phytoclast-palynomorph kerogen plot shows depositional environments of palynofacies, i.e., DFPF-A, -B, -C and SFPF A, B (based on the relative numeric frequency of organic matter).

are mainly controlled by the formation of shale (Demaison and Moore, 1980; Tyson, 1987; Wignall, 1994). However, it has been proven from recently updated studies that complicated multiple-control pathways most likely lead to the accumulation and preservation of organic matter in dark gray shale (Sageman et al., 2003; Rimmer et al., 2004; Arthur and Sageman, 2005; Bohacs et al., 2005; Wang and Carr, 2013) (Fig. 7).

In contrast to the high-potential source rock, the depositional setting of the ordinary source rock or non-high potential source rock has different parameters. The elemental ratios such as Ti/Al and Si/Al are thought to be the key proxies used to define the detrital input concentration into the basin (Werne et al., 2002; Sageman et al., 2003; Rimmer et al., 2004; Li et al., 2015). Moreover, due to the low value of Ti/Al in the high-potential source rock, the ordinary source rock has high values (7.82 on average) in most cases. The detrital influx, as defined by Cr and Ti/Al, into the basin (Soua, 2011) in ordinary rock is high compared to that in high-potential source rock. The enrichment factor of redox-sensitive elements in ordinary rock is different than that in high-potential rock, i.e., most

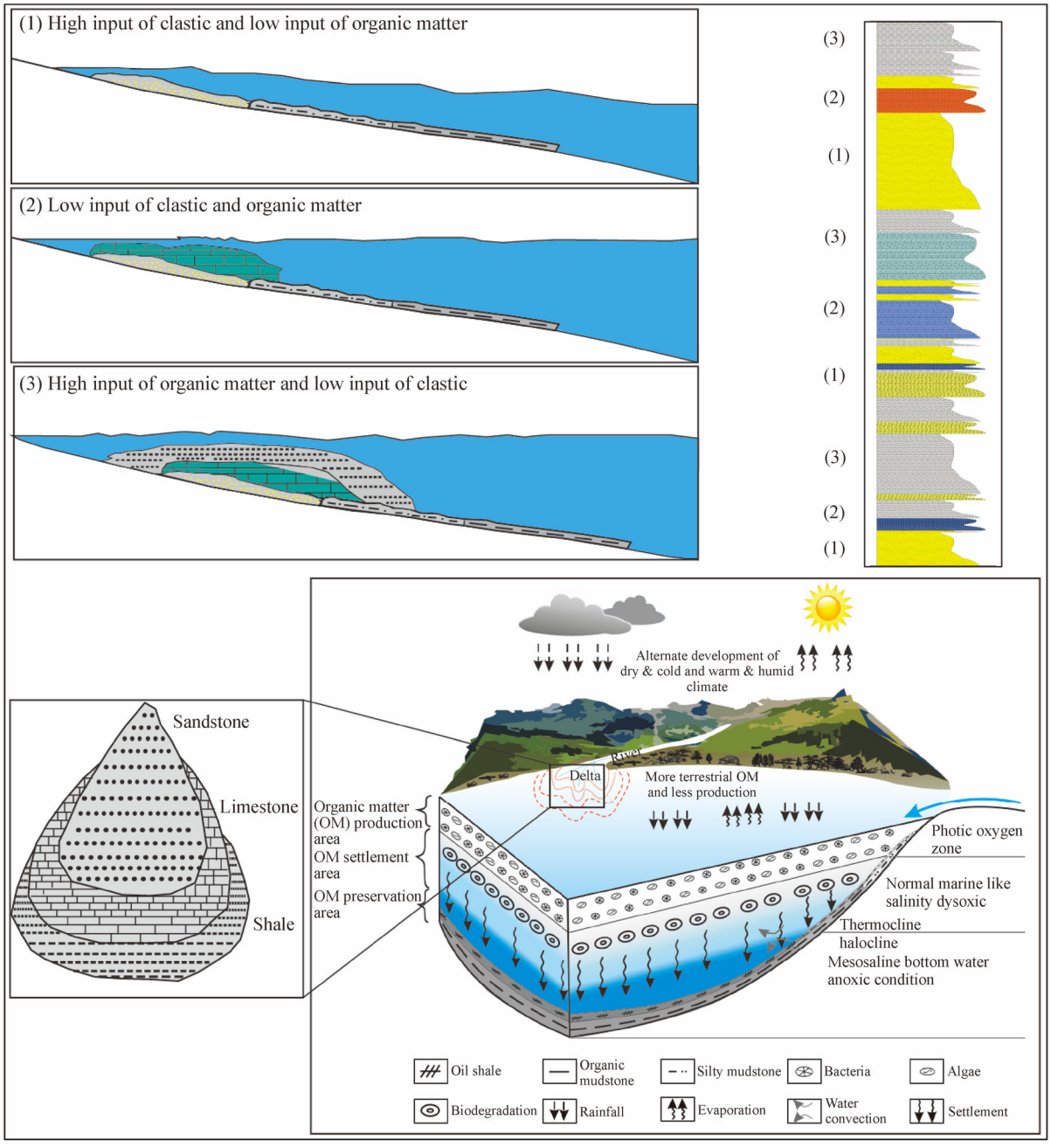

Fig. 7 The Lower to Middle Jurassic high potential shale depositional model showing the various geochemical and geological conditions for the deposition of high potential source rock in the Indus Basin, Pakistan.

are not consistently enriched. Therefore, the lack of enrichment of Cr, V, and Mo in the ordinary shale of the Lower to Middle Jurassic indicates that the deposition has taken place in oxygenated water under oxic conditions in a low anoxic setting. According to McManus et al. (2006) and Zheng et al. (2000), Mo accumulation occurred under less anoxic conditions. Thus, the bottom waters were less reducing. The V/(V + Ni) value is 0.63, and the V/(V + Cr) value is 0.47 in ordinary source rock in the Indus Basin, which supports the oxic condition of the depositional setting in Jurassic studies according to many researchers (Hatch and Leventhal, 1992; Jones and Manning, 1994; Rimmer, 2004; Baioumy and Lehmann, 2017). It has been reported that the V/Cr ratio is 1.24, and the V/Ni proxy value is 2.50, which falls in the oxic zone, suggesting a terrestrial to marine origin for this organic matter (Jones and Manning, 1994; Galarraga et al., 2008). The (Cu + Mo)/Zn value of 6.32 indicates the deposition that took place in a dysoxic geological setting (Hallberg, 1982; Jones and Manning, 1994; Gallego-Torres et al., 2010; Li et al., 2015) (Table 4). The bulk carbon and oxygen values of the non-potential source rock started with smaller $\delta^{13}C$ values of −0.1‰ compared with the pronounced anoxia in the high-potential source rock of the Lower to Middle Jurassic Indus Basin. In the ordinary source rocks, the positive excursion values are reposted from the gray shale low carbon content values in the Jurassic rocks of the Indus Basin, reflecting that anoxia is a critical factor in the formation of black shale rocks.

6 Conclusions

1) The depositional setting interpreted from the palynofacies analysis shows the deposition in a shallow marine setting.

2) The trace element analysis, carbon and oxygen isotopic study, bulk geochemical analysis and palynofacies investigation of the Lower to Middle Jurassic strata reveal that the deposition of black to gray shale took place in a dysoxic to anoxic environment with pronounced oceanic anoxic events in the proximal to the distal shelf setting.

3) The controlling factor in the deposition of high potential black shale is low detrital input, feasible reducing conditions, availability of organic matter, and deposition in a viable marine setting. The low potential source rock has more clastic input, dysoxic paleoredox conditions, less anoxia, more terrestrial organic input, and low production of primary organic matter.

4) It is concluded that complex, nonlinear relations between different aspects most likely contribute to the deposition of organic material. The enhanced preservation, pronounced anoxia, less clastic dilution with enhanced particulate sedimentary particle supply, and less primary organic marine production contribute to the deposition of shale rich in organic matter.

Acknowledgements The current research is facilitated by the Cooperation Basement of International Science and Technology on Deep Reservoir-forming Mechanism, China University of Petroleum (East China) and NCE in Geology, University of Peshawar (PSF/Res/KPK/PU/Earth (96)). We thank Professor Jin Qiang (China University of Petroleum, East China) for his support during the research process. Furthermore, the efforts of Mr. Nowrad Ali, Rahat Ullah (Department of Geology, UOP), and amateur geologist Mr. Hamza Khan Sherani during the field are worth to be mentioned and thanked for their moral, social and technical support.

References

Abbasi I A, Haneef M, Obaid S, Daud F, Qureshi A W (2012). Mesozoic deltaic system along the western margin of the Indian plate: lithofacies and depositional setting of Datta Formation, North Pakistan. Arab J Geosci, 5(3): 471–480

Abdula R A, Balaky S M, Nurmohamadi M, Piroui M (2015). Microfacies analysis and depositional environment of the Sargelu Formation (Middle Jurassic) from Kurdistan Region, northern Iraq. Donnish J Geo Mining Res, 1(1): 001–026

Ahmed S, Mertmann D, Manutsoglu E (1997). Jurassic shelf sedimentation and sequence stratigraphy of the Surghar Range, Pakistan. J Nepal Geol Soc, 15(1): 15–22

Algeo T J (2004). Can marine anoxic events draw down the trace element inventory of seawater? Geology, 32(12): 1057–1060

Algeo T J, Maynard J B (2004). Trace-element behavior and redox facies in core shales of Upper Pennsylvanian Kansas-type cyclothems. Chem Geol, 206(3–4): 289–318

Ali F, Ahmad S, Khan S, Hanif M, Qiang J (2018). Toarcian-Bathonian palynostratigraphy and anoxic event in Pakistan: an organic geochemical study. Stratigraphy, 15(3): 225–243

Ali F, Qiang J, Ahmad S, Khan S, Hanif M, Jan I U (2019). Sedimentological and geochemical analysis of the Middle Jurassic Shinawari Formation, Upper Indus Basin, Pakistan: implications for Palaeoenvironmental and hydrocarbon assessment. Arab J Sci Eng, 44(7): 6465–6487

Arthur M A, Sageman B B (2005). Sea-level control on source-rock development: perspectives from the Holocene Black Sea, the mid-Cretaceous Western Interior Basin of North America, and the Late Devonian Appalachian Basin. In: Nicholas B H, eds. The Deposition of Organic-carbon-rich Sediments: Models, Mechanisms, and Consequences. SEPM special publication 82

Baioumy H, Lehmann B (2017). Anomalous enrichment of redox-sensitive trace elements in the marine black shales from the Duwi Formation, Egypt: evidence for the late Cretaceous Tethys anoxia. J Afr Earth Sci, 133: 7–14

Baioumy H M, Ismael I S (2010). Factors controlling the compositional variations among the marine and non-marine black shales from Egypt. Int J Coal Geol, 83(1): 35–45

Bender F, Raza H A (1995). Geology of Pakistan. Cambridge: Cambridge University Press

Bohacs K M, Carroll A R, Neal J E, Mankiewicz P J (2000). Lake-basin type, source potential, and hydrocarbon character: an integrated sequence-stratigraphic-geochemical framework. In: Gierlowski-Kordesch E H, Kelts K R, eds. Lake Basins through Space and Time. AAPG Studies in Geology, 46: 3–34

Bohacs K M, Grabowski G J, Carroll A R, Mankiewicz P J, Miskell-

Gerhardt K J, Schwalbach J R, Wegner M B, Simo J T (2005). Production, destruction, and dilution—the many paths to source-rock development. SEPM Special Publications, 82: 61–101

Brumsack H J (2006). The trace metal content of recent organic carbon-rich sediments: implications for Cretaceous black shale formation. Palaeogeogr Palaeoclimatol Palaeoecol, 232(2–4): 344–361

Brumsack H J (1986). The inorganic geochemistry of Cretaceous black shales (DSDP Leg 41) in comparison to modern upwelling sediments from the Gulf of California. Geol Soc Lond Spec Publ, 21(1): 447–462

Calvert S, Pedersen T (1993). Geochemistry of recent oxic and anoxic marine sediments: implications for the geological record. Mar Geol, 113(1–2): 67–88

Calvert S, Pedersen T (2007). Elemental proxies for palaeoclimatic and palaeoceanographic variability in marine sediments: interpretation and application. Develop Marin Geo, 1: 567–644

Chen L, Yi H S, Tsai L L Y, Xu G W, Da X J, Lin A T S (2013). Jurassic black shales facies from Qiangtang Basin (northern Tibet): rare earth and trace elements for paleoceanographic implications. Acta Geol Sin (English Edition), 87(2): 540–554

Demaison G J, Moore G T (1980). Anoxic environments and oil source bed genesis. Organic Geochem, 2(1): 9–31

Dera G, Pellenard P, Neige P, Deconinck J F, Pucéat E, Dommergues J L (2009). Distribution of clay minerals in Early Jurassic Peritethyan seas: palaeoclimatic significance inferred from multiproxy comparisons. Palaeogeogr Palaeoclimatol Palaeoecol, 271(1–2): 39–51

Fatmi A, Hyderi I, Anwar M (1990). Occurrence of the Lower Jurassic ammonoid genus bouleiceras from the Surghar Range with a revised nomenclature of the Mesozoic rocks of the Salt Range and Trans Indus Ranges (Upper Indus Basin). Geol Bull Punjab U, 25: 38–46

Fürsich F, Oschmann W, Singh I, Jaitly A (1992). Hardgrounds, reworked concretion levels and condensed horizons in the Jurassic of western India: their significance for basin analysis. J Geol Soc London, 149(3): 313–331

Galarraga F, Reategui K, Martïnez A, Martïnez M, Llamas J, Márquez G (2008). V/Ni ratio as a parameter in palaeoenvironmental characterisation of nonmature medium-crude oils from several Latin American basins. J Petrol Sci Eng, 61(1): 9–14

Gallego-Torres D, Martinez-Ruiz F, De Lange G, Jimenez-Espejo F, Ortega-Huertas M (2010). Trace-elemental derived paleoceanographic and paleoclimatic conditions for Pleistocene Eastern Mediterranean sapropels. Palaeogeogr Palaeoclimatol Palaeoecol, 293(1–2): 76–89

Hallberg R (1982). Diagenetic and environmental effects on heavy-metal distribution in sediments: a hypothesis with an illustration from the Baltic Sea. In: The Dynamic Environment of the Ocean Floor. Lexington: Lexington Books, 502: 305–316

Hatch J, Leventhal J (1992). Relationship between inferred redox potential of the depositional environment and geochemistry of the Upper Pennsylvanian (Missourian) Stark Shale Member of the Dennis Limestone, Wabaunsee County, Kansas, USA. Chem Geol, 99(1–3): 65–82

Ikeda M, Hori R S, Ikehara M, Miyashita R, Chino M, Yamada K (2018). Carbon cycle dynamics linked with Karoo-Ferrar volcanism and astronomical cycles during Pliensbachian-Toarcian (Early Jurassic). Global Planet Change, 170: 163–171

Iqbal S, Wagreich M, Irfan U J, Kuerschner W M, Gier S, Bibi M (2019). Hot-house climate during the Triassic/Jurassic transition: the evidence of climate change from the southern hemisphere (Salt Range, Pakistan). Global Planet Change, 172: 15–32

Jenkyns H C (2010). Geochemistry of oceanic anoxic events. Geochem Geophys Geosyst, 11(3): Q03004

Jones B, Manning D A (1994). Comparison of geochemical indices used for the interpretation of palaeoredox conditions in ancient mudstones. Chem Geol, 111(1–4): 111–129

Kadri I (1995). Petroleum Geology of Pakistan. Islamabad: Pakistan Petroleum Limited Karachi

Kazmi A, Rana R (1982). Tectonic map of Pakistan. Islamabad: Geol Sum Pakistan

Kazmi A H, Jan M Q (1997). Geology and Tectonics of Pakistan. Islamabad: Graphic publishers

Li Y, Fan T, Zhang J, Wei X, Zhang J (2015). Impact of paleoenvironment, organic paleoproductivity, and clastic dilution on the formation of organic-rich shales: a case study about the Ordovician-Silurian black shales, southeastern Chongqing, South China. Arab J Geosci, 8(12): 10225–10239

Løseth T M, Ryseth A E, Young M (2009). Sedimentology and sequence stratigraphy of the middle Jurassic Tarbert Formation, Oseberg South area (northern North Sea). Basin Res, 21(5): 597–619

Lyons T W, Werne J P, Hollander D J, Murray R (2003). Contrasting sulfur geochemistry and Fe/Al and Mo/Al ratios across the last oxic-to-anoxic transition in the Cariaco Basin, Venezuela. Chem Geol, 195(1–4): 131–157

McLennan S M (2001). Relationships between the trace element composition of sedimentary rocks and upper continental crust. Geochem Geophys Geosyst, 2(4): 2000GC000109

McManus J, Berelson W M, Severmann S, Poulson R L, Hammond D E, Klinkhammer G P, Holm C (2006). Molybdenum and uranium geochemistry in continental margin sediments: paleoproxy potential. Geochim Cosmochim Acta, 70(18): 4643–4662

Mensink V H, Mertman D, Ahmad S (1988). Facies development during the Jurassic of the Trans Indus Ranges, Pakistan. In: Neues Jahrb Geological Paleontological memorial Germany 3: 153–166

Mertmann D, Ahmad S (1994). Shinawari and Samana Suk Formations of the Surghar and salt ranges, Pakistan: facies and depositional environments. Z Dtsch Geol Ges, 145(2): 305–317 (in German)

Moshrif M A (1987). Sedimentary history and paleogeography of Lower and Middle Jurassic rocks, central Saudi Arabia. J Pet Geol, 10(3): 335–349

Naeem K, Yawar W, Bhatti T M, Mohammad B (2011). Elemental profile of black shales. Chin J Geochem, 30(2): 217–219

Nielsen O B, Seidenkrantz M S, Abrahamsen N, Schmidt B J, Koppelhus E B, Ravn-Sørensen H, Korsbech U, Nielsen K G (2003). The Lower–Middle Jurassic of the Anholt borehole: implications for the geological evolution of the eastern margin of the Danish Basin. Geol Surv Denmark Greenl Bull, 1: 585–609

Pi D H, Jiang S Y, Luo L, Yang J H, Ling H F (2014). Depositional environments for stratiform witherite deposits in the Lower Cambrian black shale sequence of the Yangtze Platform, southern Qinling region, SW China: evidence from redox-sensitive trace element geochemistry. Palaeogeogr Palaeoclimatol Palaeoecol, 398: 125–131

Piper D, Calvert S (2009). A marine biogeochemical perspective on black shale deposition. Earth Sci Rev, 95(1–2): 63–96

Qiang J, Ming Z, Zhen L, Xianzhi G, Dehua P, Lamei L (2002). Geology and geochemistry of source rocks in the Qaidam Basin, NW China. J Pet Geol, 25(2): 219–238

Quinby-Hunt M S, Wilde P (1994). Thermodynamic zonation in the black shale facies based on iron-manganese-vanadium content. Chem Geol, 113(3–4): 297–317

Rachold V, Brumsack H J (2001). Inorganic geochemistry of Albian sediments from the Lower Saxony Basin NW Germany: palaeoenvironmental constraints and orbital cycles. Palaeogeogr Palaeoclimatol Palaeoecol, 174(1–3): 121–143

Rees P, Ziegler A M, Valdes P J, Huber B, MacLeod K, Wing S (2000). Jurassic phytogeography and climates: new data and model comparisons. Warm Climates in Earth History: 297–318

Riboulleau A, Baudin F, Deconinck J F, Derenne S, Largeau C, Tribovillard N (2003). Depositional conditions and organic matter preservation pathways in an epicontinental environment: the Upper Jurassic Kashpir Oil Shales (Volga Basin, Russia). Palaeogeogr Palaeoclimatol Palaeoecol, 197(3–4): 171–197

Rimmer S M (2004). Geochemical paleoredox indicators in Devonian–Mississippian black shales, central Appalachian Basin (USA). Chem Geol, 206(3–4): 373–391

Rimmer S M, Thompson J A, Goodnight S A, Robl T L (2004). Multiple controls on the preservation of organic matter in Devonian–Mississippian marine black shales: geochemical and petrographic evidence. Palaeogeogr Palaeoclimatol Palaeoecol, 215(1–2): 125–154

Rousseau M, Dromart G, Garcia J P, Atrops F, Guillocheau F (2005). Jurassic evolution of the Arabian carbonate platform edge in the central Oman Mountains. J Geol Soc London, 162(2): 349–362

Sageman B B, Murphy A E, Werne J P, Ver Straeten C A, Hollander D J, Lyons T W (2003). A tale of shales: the relative roles of production, decomposition, and dilution in the accumulation of organic-rich strata, Middle–Upper Devonian, Appalachian basin. Chem Geol, 195(1–4): 229–273

Scopelliti G, Bellanca A, Coccioni R, Luciani V, Neri R, Baudin F, Chiari M, Marcucci M (2004). High-resolution geochemical and biotic records of the Tethyan 'Bonarelli Level' (OAE2, latest Cenomanian) from the Calabianca–Guidaloca composite section, northwestern Sicily, Italy. Palaeogeogr Palaeoclimatol Palaeoecol, 208(3–4): 293–317

Shah M I (2009). Stratigraphy of Pakistan: Memories of Geological Survey of Pakistan. Islamabad: Ministry of Petroleum and Natural Resources of Geological Survey of Pakistan

Soua M (2011). Productivity and bottom water redox conditions at the Cenomanian-Turonian Oceanic Anoxic Event in the southern Tethyan margin, Tunisia. Mediterranean J Environ, 4: 653–664

Srivastave N, Ranawat T S (2015). An overview of Yellow Limestone deposits of the Jaisalmer Basin, Rajasthan, India. Vol Jurassica, 13(1): 107–112

Steffen D, Gorin G (1993). Palynofacies of the Upper Tithonian-Berriasian deep-sea carbonates in the Vocontian Trough (SE France). Bull Cent Rech Explor Prod Elf-Aquitaine, 17(1): 235–247

Szczepanik P, Witkowska M, Sawłowicz Z (2010). Geochemistry of Middle Jurassic mudstones (Kraków-Częstochowa area, southern Poland): interpretation of the depositional redox conditions. Geol Q, 51: 57–66

Taylor S R, McLennan S M (1985). The Continental Crust: Its Composition and Evolution. Oxford: Blackwell: 1–312

Tribovillard N, Desprairies A, Lallier-Vergès E, Bertrand P, Moureau N, Ramdani A, Ramanampisoa L (1994). Geochemical study of organic-matter rich cycles from the Kimmeridge Clay Formation of Yorkshire (UK): productivity versus anoxia. Palaeogeogr Palaeoclimatol Palaeoecol, 108(1–2): 165–181

Tribovillard N, Algeo T J, Lyons T, Riboulleau A (2006). Trace metals as paleoredox and paleoproductivity proxies: an update. Chem Geol, 232(1–2): 12–32

Tribovillard N, Lyons T, Riboulleau A, Bout-Roumazeilles V (2008). A possible capture of molybdenum during early diagenesis of dysoxic sediments. Bull Soc Geol Fr, 179(1): 3–12

Tyson R (1987). The genesis and palynofacies characteristics of marine petroleum source rocks. Geol Soc Lond Spec Publ, 26(1): 47–67

Tyson R (1995). Abundance of organic matter in sediments: TOC, hydrodynamic equivalence, dilution and flux effects. In: Sedimentary Organic Matter. Berlin: Springer: 81–118

Usman M, Siddiqui N A, Zhang S, Ramkumar M, Mathew M, Sautter B, Beg M A (2020a). Ichnofacies and sedimentary structures: a passive relationship with permeability of a sandstone reservoir from NW Borneo. J Asian Earth Sci, 192: 103992

Usman M, Zhang S, Siddiqui N A, Jamal J (2020b). The influential parameters of the reservoir quality of Sandakan sandstone, NW Borneo. In: 2nd SEG Rock Physics Workshop: Challenges in Deep and Unconventional Oil/Gas Exploration, Soc of Exp Geophys, 8–11

Usman M, Siddiqui N A, Mathew M, Zhang S, El-Ghali M A, Ramkumar M, Jamil M, Zhang Y (2020c). Linking the influence of diagenetic properties and clay texture on reservoir quality in sandstones from NW Borneo. Mar Pet Geol, 120: 104509

Vine J D, Tourtelot E B (1970). Geochemistry of black shale deposits; a summary report. Econ Geol, 65(3): 253–272

Wang G, Carr T R (2013). Organic-rich Marcellus Shale lithofacies modeling and distribution pattern analysis in the Appalachian Basin organic-rich shale lithofacies modeling, Appalachian Basin. Am Assoc Pet Geol Bull, 97(12): 2173–2205

Waples D W (1983). Reappraisal of anoxia and organic richness, with emphasis on Cretaceous of North Atlantic. Am Assoc Pet Geol Bull, 67(6): 963–978

Wedepohl K (1971). Environmental influences on the chemical composition of shales and clays. Phys Chem Earth, 8(1): 307–333

Wedepohl K (1991). The composition of the upper earth's crust and the natural cycles of selected metals; metals in natural raw materials. In: Natural Resources. Weinheim: VCH

Werne J P, Sageman B B, Lyons T W, Hollander D J (2002). An integrated assessment of a "type euxinic" deposit: evidence for multiple controls on black shale deposition in the Middle Devonian Oatka Creek Formation. Am J Sci, 302(2): 110–143

Wignall P B (1994). Black Shales. Oxford: Oxford University Press

Wood G, Gabriel A, Lawson J (1996). Palynological techniques-processing and microscopy. In: Palynology: Principles and Applications, 1: 29–50. American Association of Stratigraphic Palynologist

Yang J, Jiang S, Ling H, Feng H, Chen Y, Chen J (2004).

Paleoceangraphic significance of redox-sensitive metals of black shales in the basal Lower Cambrian Niutitang Formation in Guizhou Province, south China. Prog Nat Sci, 14(2): 152–157

Yang Y, Ritts B, Zou C, Xu T, Zhang B, Xi P (2003). Upper Triassic-Middle Jurassic stratigraphy and sedimentology in the NE Qaidam Basin, NW China: petroleum geological significance of new outcrop and subsurface data. J Pet Geol, 26(4): 429–449

Zheng D, Miska S, Ziaja M, Zhang J (2019). Study of anisotropic strength properties of shale. AGH Drilling Oil Gas 36(1): 93–111

Zheng Y, Anderson R F, Van Geen A, Kuwabara J (2000). Authigenic molybdenum formation in marine sediments: a link to pore water sulfide in the Santa Barbara Basin. Geochim Cosmochim Acta, 64(24): 4165–4178